Research Article

Structure and electrical properties of lead-free $(1-x)(K_{0.45}Na_{0.5}Li_{0.05})Nb_{0.95}Sb_{0.05}O_3 - x(Ca_{0.95}Ba_{0.05})(Zr_{0.9}Sn_{0.1})O_3$ ceramics

Yunhe Yi[1] · Yang Lu[1] · Jinchuan Wang[1] · Xudong Bai[1] · Yongqi Pan[1] · Yungang Yu[1] · Caiwang He[1] · Yunyi Liu[1] · Yi Chen[1,2]

Received: 31 January 2020 / Accepted: 19 March 2020 / Published online: 29 March 2020

Abstract
Lead-free perovskite piezoelectric $(1-x)(K_{0.45}Na_{0.5}Li_{0.05})Nb_{0.95}Sb_{0.05}O_3 - x(Ca_{0.95}Ba_{0.05})(Zr_{0.9}Sn_{0.1})O_3$ ceramics were fabricated via a conventional sintering process. A microstructural study was conducted for the ceramics through a scanning electron microscope, whose grain sizes were found to gradually reduce with increasing x. The phase structure of the studied ceramics was identified by the combined analysis of X-ray diffraction data and dielectric-temperature measurements, and a rhombohedral–orthorhombic–tetragonal phase coexistence was observed to exist in the wide composition range of $0 \le x \le 0.05$. The ceramics exhibited the optimal piezoelectric properties at $x = 0.01$, which had a piezoelectric constant d_{33} of 290 pC/N and a planar electromechanical coupling coefficient of 0.43. A diffuse phase transition was induced with x increased to a relatively high value, featuring the broadening of Curie peak. In addition, the variations of ferroelectric properties with composition were investigated in this work as well. The authors believe that adding the calcium barium zirconate stannate compound $(Ca_{0.95}Ba_{0.05})(Zr_{0.9}Sn_{0.1})O_3$ into $(K,Na)NbO_3$-based ceramics is a valid way for the improvement of their piezoelectric properties.

Keywords Lead-free ceramics · Alkali metal niobates · Perovskites · Dielectric properties · Piezoelectric properties · Phase coexistences

1 Introduction

$(K,Na)NbO_3$ (KNN)-based ceramics are extensively regarded to be among the most potential lead-free candidates for the replacement of toxic $Pb(Zr_{1-x}Ti_x)O_3$ (PZT)-based piezoelectric materials, due to their prominent electrical properties and high Curie temperature (T_C) of ~ 410 °C [1–4]. Many commercial PZT-based ceramics lie at a composition near the morphotropic phase boundary (MPB) separating the rhombohedral and tetragonal phases [5], as the two-phase coexistence in the MPB is able to make the domains reorient easier during poling and thereby results in a significant enhancement of piezoelectric activity. There also exist phase boundaries in KNN-based solid solutions, which exhibit a similar enhancing effect on the piezoelectric activity like the MPB in PZT [6–9]. The earliest constructed phase boundary in KNN-based ceramics was orthorhombic–tetragonal (O–T) phase boundary, following by rhombohedral–orthorhombic (R–O) phase boundary [10]. The two kinds of phase boundaries correspond to the R–O and O–T phase transitions of pure KNN, respectively, and the formation of an R–O or O–T phase boundary is through shifting the temperature of the corresponding phase transition (i.e., the T_{R-O} or T_{O-T}) to room temperature [10–12]. Unfortunately, the KNN-based ceramics with one of such two kinds of

✉ Yi Chen, mrchenyi@swu.edu.cn | [1]School of Materials and Energy, Southwest University, Chongqing 400715, People's Republic of China. [2]National and Local Joint Engineering Laboratory of Intelligent Transmission and Control Technology (Chongqing), Southwest University, Chongqing 400715, People's Republic of China.

SN Applied Sciences (2020) 2:775 | https://doi.org/10.1007/s42452-020-2574-x

phase boundaries are far inferior in piezoelectric properties to the PZT-based ceramics near the MPB.

Over recent years, piezoelectric properties comparable to that of practical PZT-based materials have been achieved in KNN-based ceramics by constructing a rhombohedral to tetragonal (R–T) phase boundary [13–17], which consists of the same two phases as the MPB of PZT. It is by merging the T_{R-O} and T_{O-T} of KNN into one temperature, usually room temperature, that the R–T phase boundary is constructed [13–17]. However, it is recently found that the so-called R–T phase boundary in many ceramic systems actually possesses a three-phase coexistence of R–O–T phases [18]. It is reported that adding the right amount of Li^+ ions into KNN will move the T_{O-T} to room temperature [9], while the Sb^{5+} ions substitution can increase the T_{R-O} [19]. Therefore, the Li^+ and Sb^{5+} ions as dopants are both very useful for the construction of R–O–T phase boundary. Some ABO_3-type compounds, such as $AZrO_3$ (A = Ba, Ca and Sr, etc.), are capable of simultaneously shifting the T_{R-O} and T_{O-T} to room temperature [20–23], and thus can greatly benefit the establishment of R–O–T phase boundary. For example, an R–O–T phase boundary was successfully formed in our previously studied KNN-based ceramics modified with $CaZrO_3$ [24]. However, the R–O–T phase boundary usually exists in an extremely narrow composition range, which makes the piezoelectric activity of the corresponding ceramic system exhibit a strong compositional dependence, and this is very disadvantageous for large-scale production.

It is found that the R–O–T phases can coexist within a relatively wide composition range after adding a suitable amount of $BaZrO_3$ into KNN-based ceramics [25]. Additionally, Sn^{4+} substitution for partial Zr^{4+} in Zr-containing KNN-based ceramics reportedly can effectively improve the piezoelectric properties [26]. Therefore, a novel lead-free piezoelectric system, with the formula of $(1-x)(K_{0.45}Na_{0.5}Li_{0.05})Nb_{0.95}Sb_{0.05}O_3 - x(Ca_{0.95}Ba_{0.05})(Zr_{0.9}Sn_{0.1})O_3$ [abbreviated as: $(1-x)$KNLNS-xCBZS], was developed in this current work. Dense microstructures were obtained by preparing the ceramics using a conventional sintering process. The effect of CBZS content on the phase structure of the solid solution system was investigated, and an R–O–T phase boundary was found to exist in a wide composition range of $0 \le x \le 0.05$, which is very positive for practical use.

2 Experimental procedure

2.1 Preparation process

In this study, the $(1-x)$KNLNS-xCBZS ceramic samples with $x = 0$ to 0.07 were fabricated by a conventional solid-oxide technique. The used raw materials consisted of K_2CO_3 (99%), Na_2CO_3 (99.8%), Li_2CO_3 (98%), Nb_2O_5 (99.5%), Sb_2O_3 (99.5%), $CaCO_3$ (99%), $BaCO_3$ (99%), ZrO_2 (99%) and SnO_2 (99.8%) powders. All the raw materials were weighed stoichiometrically except for alkali metal carbonates, which were added in an excess of 0.5 wt% over the stoichiometric quantity to compensate the volatilization during sintering. These starting powders were then poured into a nylon jar with a moderate amount of ethanol. The jar rolled on a ball mill for 24 h to well mix the raw materials, using ZrO_2 balls as medium. The slurry was dried and then pre-sintered at 850 °C for 6 h. The pre-sintered powders were ground and crushed again, and subsequently were compacted into pellets of ~ 1 mm in thickness and ~ 10 mm in diameter after granulation using a polyvinyl alcohol (PVA) binder. Following a removal of the PVA at 500 °C for 2 h, the green body pellets of each composition were air-sintered at, at least, three different temperatures for 3 h, and only the ceramic samples sintered at the optimal sintering temperature were used for subsequent characterization. The optimal sintering temperatures of the compositions $x = 0$, 0.01, 0.02, 0.03, 0.04, 0.05 and 0.07 were 1080, 1065, 1080, 1120, 1120, 1150 and 1150 °C, respectively. The samples for electrical characterization were firstly polished to obtain parallel surfaces, and subsequently were coated with a post-fired silver paste on both sides of them to act as electrodes, and finally were fired at 600 °C to ensure a good bonding between the electrode and the ceramic surface.

2.2 Characterization techniques

The surface micrographs of the ceramic samples were observed via a scanning electron microscope (SEM), and their phase structures were identified by an X-ray diffraction (XRD) method in a continuous scan mode. A computer-controlled precision LCR meter was employed to test the relative dielectric constants (ε_r) of the ceramics in the temperature range from about − 100 to 150 °C and from room temperature to 450 °C, which were beforehand placed in a specially designed heating chamber. For the characterization of piezoelectric properties, a dc field of around 4 kV/mm was applied on the ceramic samples immersed in a room-temperature silicon oil bath for 30 min. After aging the polarized ceramic samples in air for at least 24 h, their piezoelectric constants d_{33} were measured on a quasi-static d_{33} meter, and the planar electromechanical coupling coefficients (k_p) were determined by a resonance–antiresonance method. A ferroelectric test system was employed to measure the polarization versus electric field (P–E) hysteresis loops of the ceramic samples placed in silicone oil.

3 Results and discussion

3.1 Surface morphology

Figure 1 shows the SEM surface micrographs of (1 − *x*) KNLNS-*x*CBZS ceramics with different CBZS contents, all of which exhibit a dense morphology with few pores. In addition, the grains of all the compositions can be found mainly in the shape of a cuboid, which is a typical microstructure of KNN-based ceramics fabricated by conventional sintering method [8, 25, 26]. The pure KNLNS ceramic sample shows a relatively uniform distribution in grain size, while the CBZS-modified ceramics present a bimodal distribution that the small grains are randomly distributed between the large ones, just like frequently observed in many other Zr-containing KNN-based ceramics [21, 22, 27].

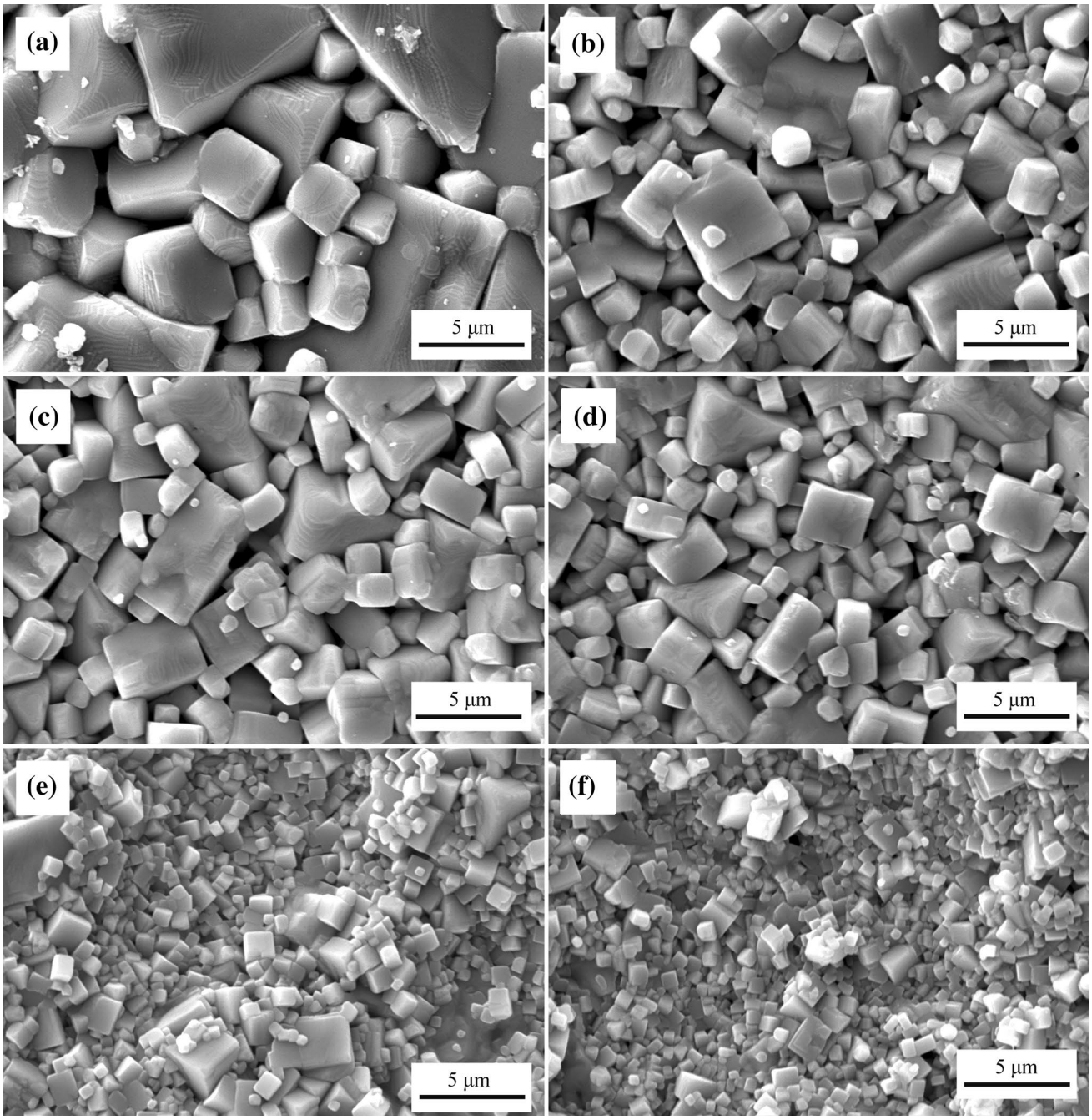

Fig. 1 SEM surface microstructures of (1 − *x*)KNLNS-*x*CBZS ceramics with **a** *x* = 0, **b** *x* = 0.01, **c** *x* = 0.02, **d** *x* = 0.03, **e** *x* = 0.04 and **f** *x* = 0.05

It is well-known that grain size plays an important role in the electrical properties of KNN-based ceramics, and hence the grain size statistics of (1 − *x*)KNLNS-*x*CBZS ceramics are calculated, adopting the method described in Ref.[28], and summarized in Fig. 2. Additionally, each panel in Fig. 2 also presents the average grain size of each corresponding ceramic sample, estimated in the light of the Heyn Lineal Intercept Procedure proposed in ASTM E112-96 standard. One can note a decreasing trend of the grain size with increase in the CBZS content, and the average grain size decreases from ~ 4.2 μm of pure KNLNS to ~ 0.8 μm of the composition $x = 0.05$. This indicates that CBZS incorporation suppresses the growth of grains during sintering, which can be explained as follows: the ions contained in CBZS have a finite ability to diffuse into the grain interior, due to the large differences between them and the cations of KNLNS in not only valence but also ionic radius, and hence these ions are liable to accumulate at the grain boundaries, thereby forming a barrier to the movement of grain boundary at high temperatures.

The density (or porosity) also has a critical impact on the electrical properties of piezoelectric ceramics. In this work, the porosities of (1 − *x*)KNLNS-*x*CBZS ceramics were determined based on the SEM images using the Image-Pro plus 6.0 software, as shown in Fig. 3. It is found that all the compositions have a porosity of around 4% except for $x = 0.07$, whose porosity is up to 8%.

3.2 Phase structure analysis

Figure 4a displays the XRD images from $2\theta = 20°$ to 60° of (1 − *x*)KNLNS-*x*CBZS ceramics, measured at room temperature. All the XRD peaks can be attributed to perovskite structure, implying that the CBZS has diffused into the lattice of KNLNS within the studied composition range. The regions between 43° and 47° of the XRD patterns are enlarged and shown in Fig. 4b, for better observation of the structural variations of the ceramics. It can be viewed that there obviously are two divided peaks at around 45° for the ceramics with a low CBZS content, which can be indexed as (002) and (200) reflections, respectively. The two divided peaks tend to approach to each other upon increasing *x* and finally merge into a single one at $x = 0.07$. The complete merging of the (002) and (200) peaks is an indication that the composition $x = 0.07$ possesses a pure rhombohedral structure, as suggested by Refs.[29, 30]. It is to be noted that the shape of the (200) peak is distinctly asymmetrical for the compositions $x = 0.04$ and 0.05, indicating that the peak is actually not a real single peak. Therefore, a multiphase structure containing the rhombohedral phase can be expected to exist below $x = 0.07$.

The temperature-dependent dielectric constants (ε_r) have been measured from about − 100 °C to 150 °C for further identification of the phase structure of (1 − *x*) KNLNS-*x*CBZS ceramics, as illustrated in Fig. 5. It is extensively known that there exist two phase transitions below T_C in pure KNN, namely, the R–O and O–T phase transitions, as introduced in Sect. 1. Therefore, there are usually two dielectric anomalies on the dielectric-temperature curves of KNN-based ceramics in addition to the Curie peak, which correspond to the R–O and O–T phase transitions, respectively. However, only one anomaly can be seen on the dielectric-temperature curves of the ceramics with $x = 0$ to 0.05, and this implies that their R–O and O–T phase transitions have merged into an R–O–T phase coexistence, as indicated by many Refs [13–17]. The temperatures of the R–O–T phase coexistence (T_{R-O-T}) are all near the room temperature, suggesting that these above-mentioned compositions possess a structure of R–O–T phase coexistence at room temperature. The R–O–T phase coexistence, also known as R–O–T phase boundary, has played an important role in the improvement of piezoelectric activity in KNN-based ceramics [13–18], and therefore it is highly positive that the R–O–T phases coexist in such a wide composition range as in this work. The R–O–T dielectric anomaly finally disappears at $x = 0.07$, owing to the formation of a pure rhombohedral structure.

3.3 Characteristics of ferroelectric-paraelectric phase transition

Figure 6 demonstrates the dielectric-temperature curves of the unpolarized (1 − *x*)KNLNS-*x*CBZS ceramics from room temperature to 450 °C, in order to study their ferroelectric-paraelectric phase transition. The peaks on these curves are widely known to be associated with the ferroelectric-paraelectric phase transition, and their temperatures are generally determined as the T_C. The T_C, together with the T_{R-O-T} obtained from Fig. 5, is plotted in Fig. 7 as a function of CBZS content. One can notice that the ε_r at the Curie peak (i.e., the maximum permittivity) and the T_C both tend to decline with the increase of CBZS content. Nevertheless, the T_C is still much above room temperature even for $x = 0.07$. This verifies the previous deduction that the composition $x = 0.07$ belongs to a ferroelectric rhombohedral structure rather than a paraelectric cubic structure.

The addition of CBZS is also found to result in an obvious broadening of the Curie peak from Fig. 6, especially for the ceramics with a relatively high CBZS content, which clearly show the characteristics of diffusion phase transition. A modified Curie–Weiss law, proposed by Uchino and Nomura [31], can be used to empirically determine the degree of diffuseness:

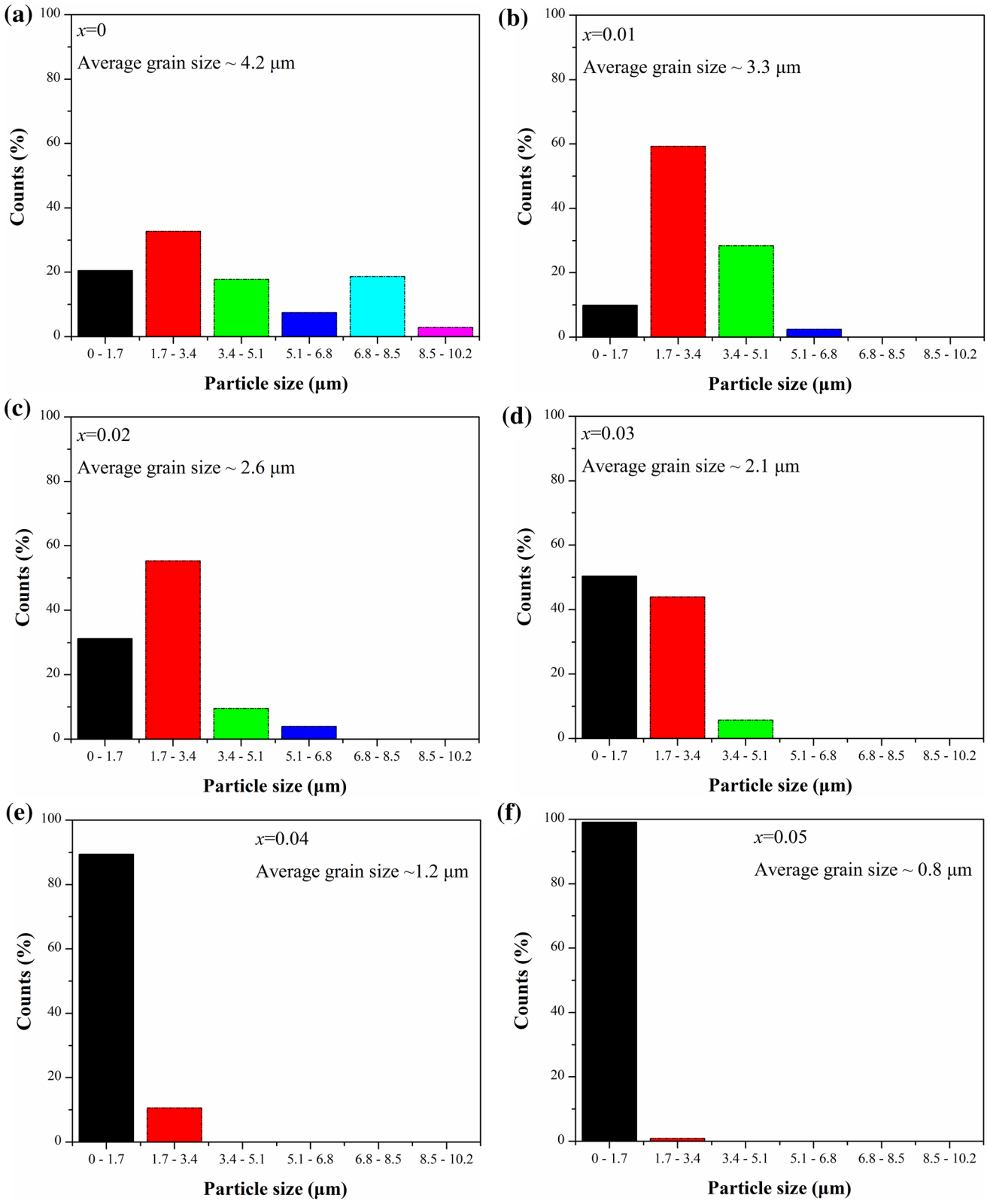

Fig. 2 Grain size distributions of (1 − *x*)KNLNS-*x*CBZS ceramics with **a** *x* = 0, **b** *x* = 0.01, **c** *x* = 0.02, **d** *x* = 0.03, **e** *x* = 0.04 and **f** *x* = 0.05

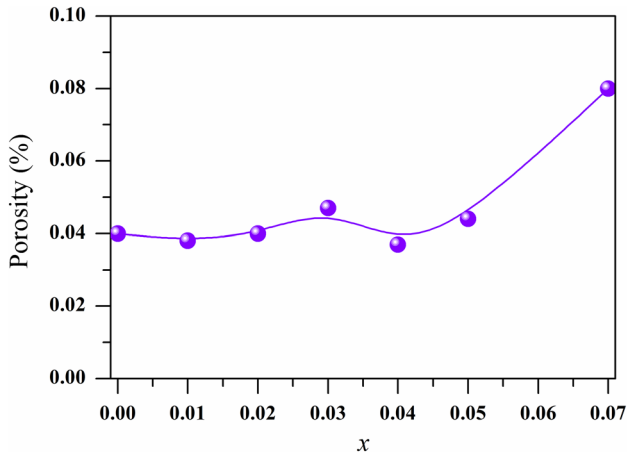

Fig. 3 Porosity of (1 − *x*)KNLNS–*x*CBZS ceramics as a function of *x*

$$\frac{1}{\varepsilon} - \frac{1}{\varepsilon_m} = \frac{(T - T_m)^{\gamma}}{C} \quad (1)$$

where ε_m and T_m are the maximum dielectric constant and the corresponding temperature, and *C* refers to the Curie-like constant, while the notation *γ* is an exponent that highly correlates with the degree of diffuseness. The *γ* value ranges from 1 of a normal ferroelectric to 2 of an ideal relaxor ferroelectric. Figure 8 plots the $\ln\left(\frac{1}{\varepsilon} - \frac{1}{\varepsilon_m}\right)$ as a function of $\ln(T - T_m)$ for (1 − *x*)KNLNS-*x*CBZS ceramics. The *γ* value, which is determined from the slope of the fitting straight lines, can be found tending to increase with the addition of CBZS. It is the polar nano regions (PNRs) created by chemically inhomogeneous micro-regions [32] that lead to the diffuseness of the Curie transition, as suggested by Refs.[33, 34]. In this study, adding CBZS will inevitably cause a large compositional inhomogeneity in the ceramics, owing to the large differences between CBZS and KNLNS as mentioned in Sect. 3.1, and consequently the diffusion phase transition is induced as the CBZS addition rises to a relatively high amount.

3.4 Room-temperature electrical properties

Figure 9a illustrates the piezoelectric constant d_{33} and planar electromechanical coupling coefficient (k_p) of the poled (1 − *x*)KNLNS-*x*CBZS ceramics as functions of *x*. One can note that the d_{33} and k_p exhibit the same trend with increasing *x*, and both of them maintain relatively high values in the wide composition range $0 \le x \le 0.05$. It is the R–O–T phase boundary formed in these compositions that contributes to the excellent piezoelectric properties, as the phase boundary can bring about more possible polarization states [35]. The maximum d_{33} and k_p values both occur at $x = 0.01$, with $d_{33} = 290$ pC/N and $k_p = 0.43$. The d_{33} and k_p then incline to slightly decrease with increasing *x* within the composition range $0.02 \le x \le 0.05$, though these compositions still have a structure of R–O–T phase coexistence. The slight declination in their piezoelectric properties may be ascribed to

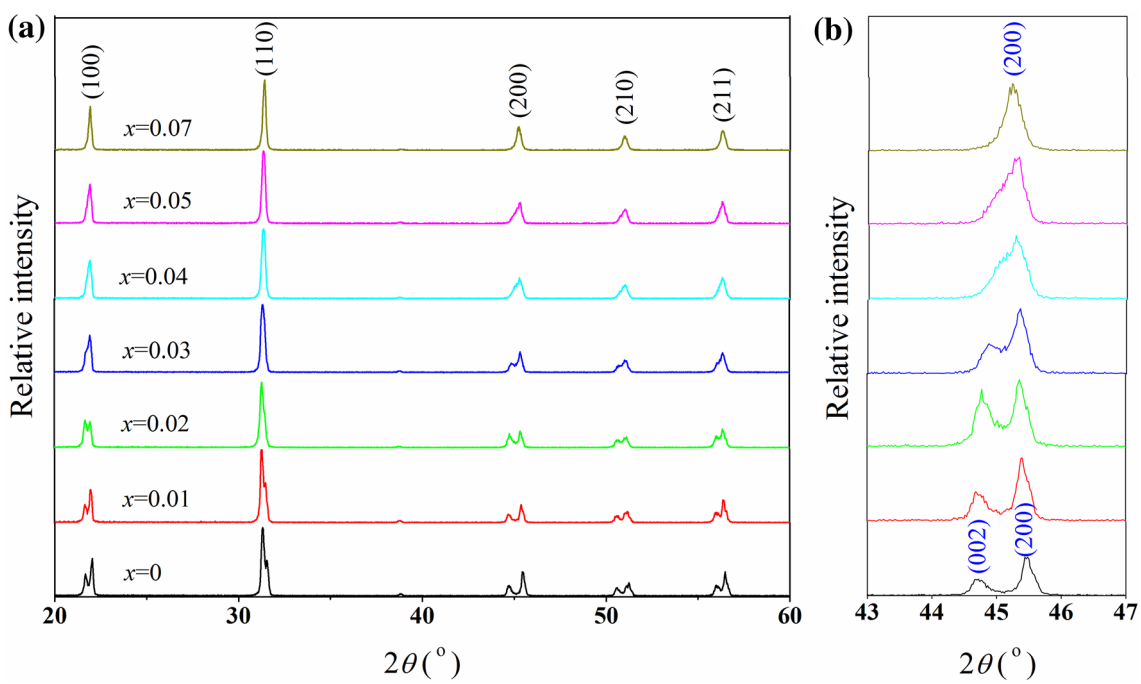

Fig. 4 XRD images of (1 − *x*)KNLNS–*x*CBZS ceramics in the 2*θ* range **a** 20–60° and **b** 43–47°

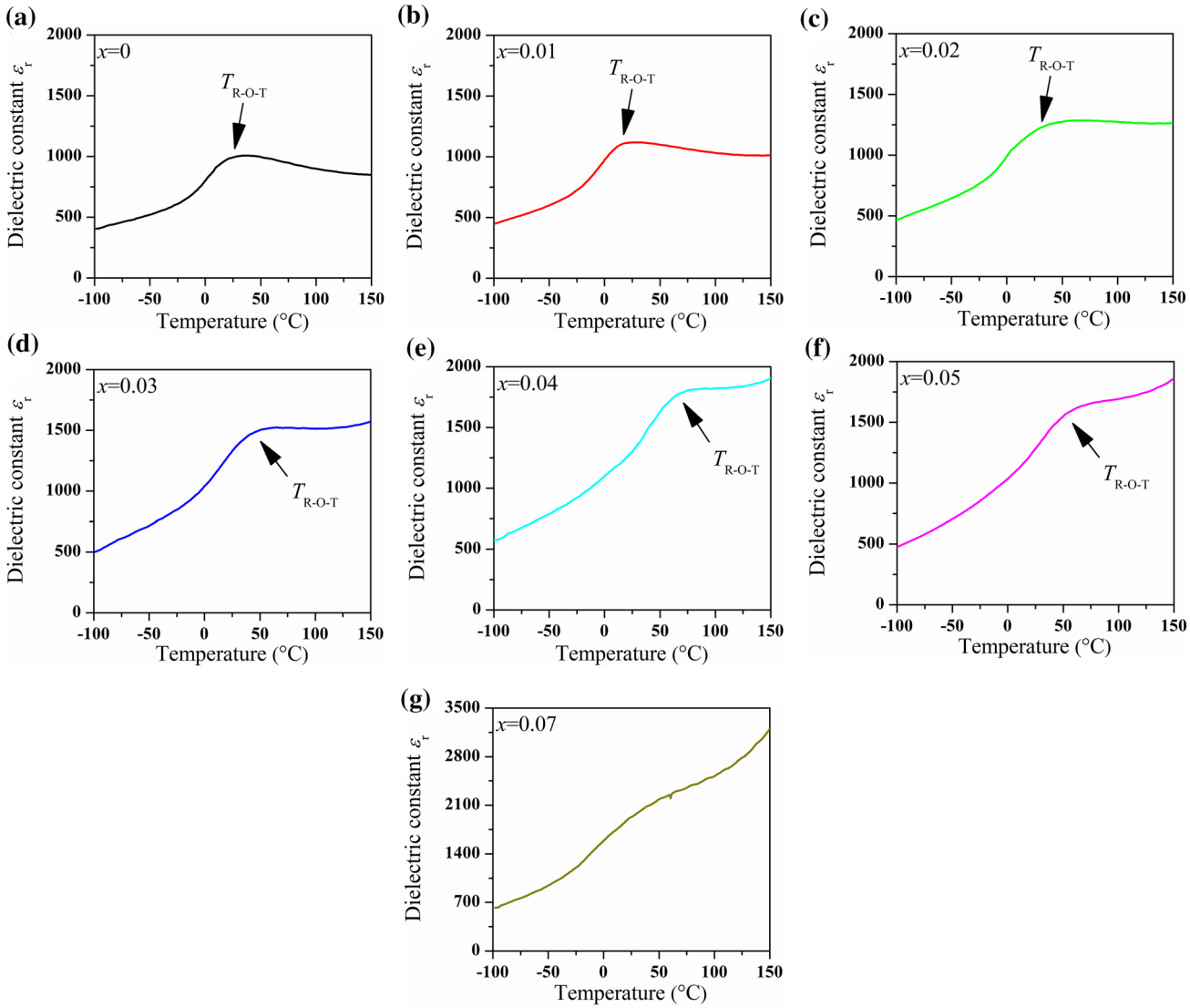

Fig. 5 Temperature dependence of dielectric constant of the (1 − *x*)KNLNS-*x*CBZS ceramics with **a** *x* = 0, **b** *x* = 0.01, **c** *x* = 0.02, **d** *x* = 0.03, **e** *x* = 0.04, **f** *x* = 0.05 and **g** *x* = 0.07, measured in the temperature range from about − 100 °C to 150 °C and at 10 kHz

the inhibited grain growth during sintering, as discussed in Sect. 3.1. In addition, the T_{R-O-T} raised to somewhat above room temperature, as demonstrated in Fig. 7, are partly responsible for the reduced piezoelectric activity of these compositions as well. With the structure transforming from an R–O–T phase coexistence to a single rhombohedral phase at *x* = 0.07, both the d_{33} and k_p experience a dramatic reduction.

Figure 9b shows the dependences of dielectric constant ε_r and loss tgδ (both measured at 10 kHz) on the composition. The ε_r is seen to show a nearly continuous increase with CBZS content, which is similar to its variation with $BaZrO_3$ content as observed in $BaZrO_3$-modified KNN-based ceramics [22]. Furthermore, it is noticed that the tgδ of the composition *x* = 0.07 is much larger than that of other compositions, and this can be attributed to its high porosity.

3.5 Ferroelectric properties

The *P*–*E* hysteresis loops of (1 − *x*) KNLNS-*x*CBZS ceramics were measured at 10 Hz to investigate their ferroelectric properties, as illustrated in Fig. 10. The pure KNLNS is observed to exhibit a roundish hysteresis loop, indicating that a large leakage current was generated during the measuring cycle. This should mainly be ascribed to the volatilization of alkali metal cations, which leads to the production of many vacancies in the lattice [10]. In addition, the pores in the ceramics are also responsible for the generation of leakage current, as there are generally a lot of

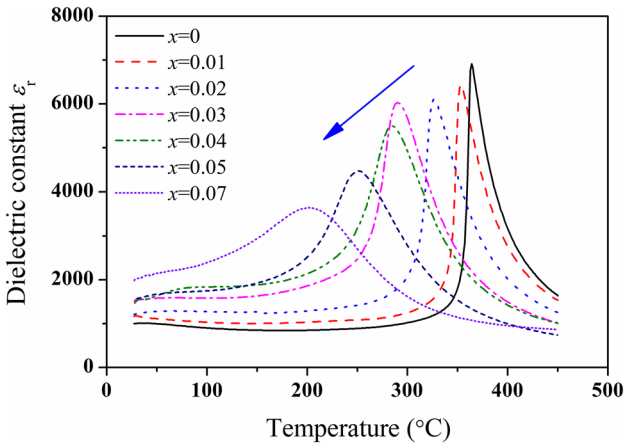

Fig. 6 Temperature dependence of dielectric constant of the (1 –*x*) KNLNS-*x*CBZS ceramics, measured in the temperature range from room temperature to 450 °C and at 10 kHz

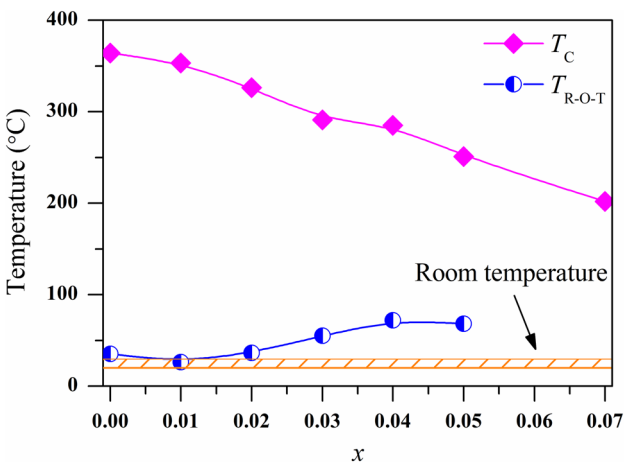

Fig. 7 T_C and $T_{R–O–T}$ of (1 – *x*)KNLNS-*x*CBZS ceramics as functions of *x*

space charges around the pores. Relatively square hysteresis loops are observed for these CBZS-modified ceramics, implying that the addition of CBZS into the ceramics can give rise to a substantial reduction in leakage current density. Moreover, one can notice that there are little changes in the remanent polarization (P_r) for all the R–O–T phase coexistence compositions, except for the pure KNLNS, whose P_r value cannot be accurately estimated owing to its irregular loop shape.

4 Conclusions

The lead-free perovskite piezoelectric (1 – *x*)KNLNS-*x*CBZS ceramics have been successfully prepared utilizing a conventional sintering technique. The addition of CBZS into the ceramics causes a reduction in grain size on account of its inhibiting impact on the grain growth during sintering. A rhombohedral-orthorhombic-tetragonal phase boundary has been formed in a wide composition range $0 \le x \le 0.05$ for the studied ceramic system. As *x* increases to 0.07, the three-phase coexistence structure is then transformed into a single rhombohedral structure. The optimal piezoelectric properties are achieved at $x = 0.01$, whose d_{33} and k_p are 290 pC/N and 0.43, respectively. To sum up, adding a suitable amount of CBZS into KNN-based ceramics is a valid way for the construction of rhombohedral-orthorhombic-tetragonal phase boundary, and accordingly can bring about the considerable enhancement of piezoelectric properties.

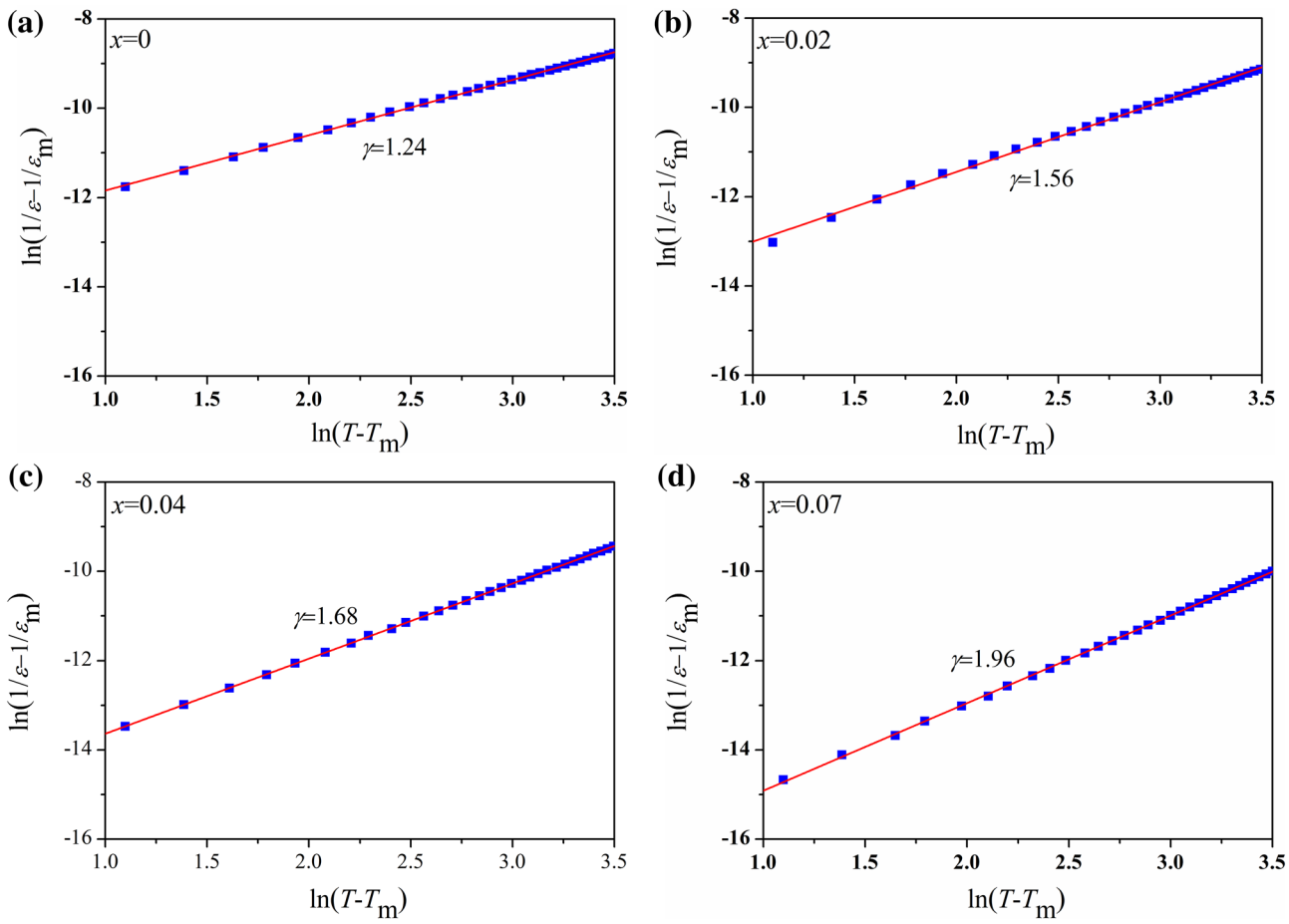

Fig. 8 The plots of $\ln(1/\varepsilon - 1/\varepsilon_m)$ as a function of $\ln(T - T_m)$ for the $(1 - x)$KNLNS-xCBZS ceramics

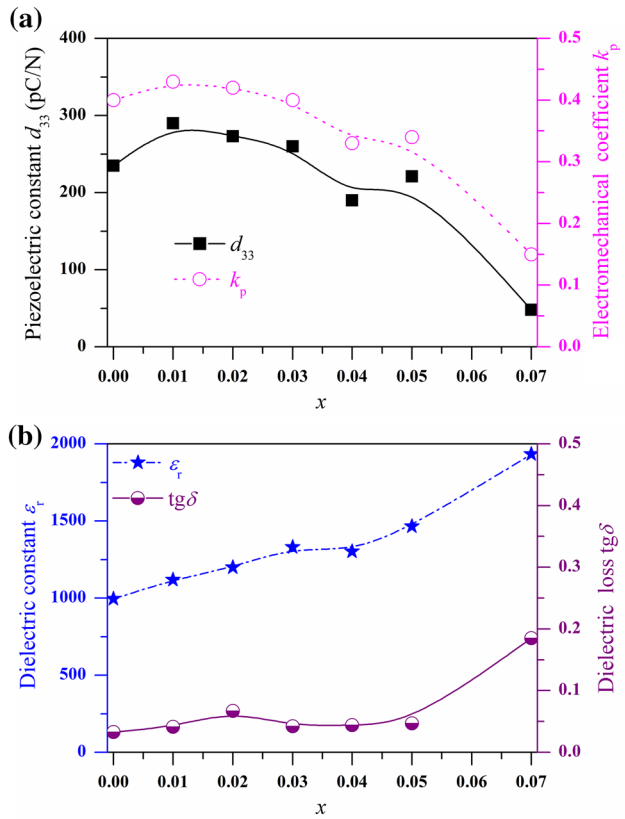

Fig. 9 **a** d_{33} and k_p and **b** ε_r and tgδ of the poled (1 − *x*)KNLNS-*x*CBZS ceramics as functions of *x*

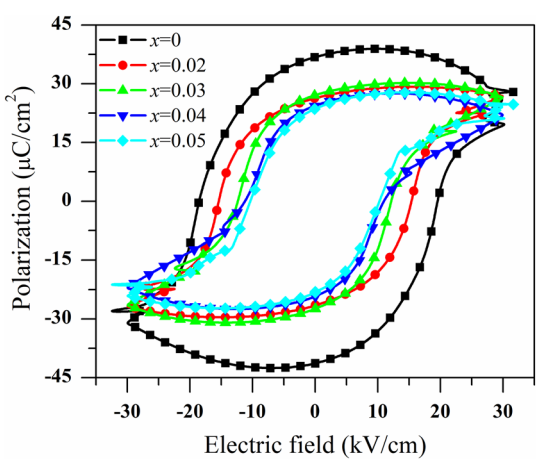

Fig. 10 Ferroelectric hysteresis loops of (1 − *x*)KNLNS-*x*CBZS ceramics with different CBZS contents

Acknowledgements This work was supported by Fundamental Research Funds for the Central Universities (No. XDJK2020B003) and "Zeng Sumin Cup" Research Project (No. zsm20190623) of School of Materials and Energy, Southwest University, China. The authors are also grateful for the grant support provided by the Undergraduate Innovation and Entrepreneurship Training Programs of Chongqing Municipality (No. S201910635069) and Southwest University (No. X201910635281).

Compliance with ethical standards

Conflict of interest On behalf of all authors, the corresponding author states that there is no conflict of interest.

References

1. Wu J (2018) Advances in lead-free piezoelectric materials. Springer, Singapore
2. Zheng T, Wu J, Xiao D, Zhu J (2018) Recent development in lead-free perovskite piezoelectric bulk materials. Prog Mater Sci 98:552–624
3. Rödel J, Webber KG, Dittmer R, Jo W, Kimura M, Damjanovic D (2015) Transferring lead-free piezoelectric ceramics into application. J Eur Ceram Soc 35:1659–1681
4. Shrout TR, Zhang SJ (2007) Lead-free piezoelectric ceramics: alternatives for PZT. J Electroceram 19:111–124
5. Jaffe B, Cook WR Jr, Jaffe H (1971) Piezoelectric ceramics. Academic Press, New York
6. Wang R, Bando H, Katsumata T, Inaguma Y, Taniguchi H, Itoh M (2009) Tuning the orthorhombic-rhombohedral phase transition temperature in sodium potassium niobate by incorporating barium zirconate. Phys Status Solidi RRL 3:142–144
7. Du H, Zhou W, Luo F, Zhu D, Qu S, Pei Z (2007) Perovskite lithium and bismuth modified potassium–sodium niobium lead-free ceramics for high temperature applications. Appl Phys Lett 91:182909
8. Lin D, Kwok KW, Lam KH, Chan HLW (2007) Structure and electrical properties of $K_{0.5}Na_{0.5}NbO_3$–$LiSbO_3$ lead-free piezoelectric ceramics. J Appl Phys 101:074111
9. Guo Y, Kakimoto K, Ohsato H (2004) Phase transitional behavior and piezoelectric properties of $(Na_{0.5}K_{0.5})NbO_3$–$LiNbO_3$ ceramics. Appl Phys Lett 85:4121–4123
10. Wu J, Xiao D, Zhu J (2015) Potassium–sodium niobate lead-free piezoelectric materials: past, present, and future of phase boundaries. Chem Rev 115:2559–2595
11. Wang K, Malič B, Wu J (2018) Shifting the phase boundary: potassium sodium niobate derivates. MRS Bull 43:607–611
12. Xing J, Zheng T, Wu J, Xiao D, Zhu J (2018) Progress on the doping and phase boundary design of potassium–sodium niobate lead-free ceramics. J Adv Dielectr 8:1830003
13. Zheng T, Zhang Y, Ke Q, Wu H, Heng LW, Xiao D, Zhu J, Pennycook SJ, Yao K, Wu J (2020) High-performance potassium sodium niobate piezoceramics for ultrasonic transducer. Nano Energy 70:104559
14. Zheng T, Wu H, Yuan Y, Lv X, Li Q, Men T, Zhao C, Xiao D, Wu J, Wang K, Li J, Gu Y, Zhu J, Pennycook SJ (2017) The structural origin of enhanced piezoelectric performance and stability in lead free ceramics. Energy Environ Sci 10:528–537
15. Xu K, Li J, Lv X, Wu J, Zhang X, Xiao D, Zhu J (2016) Superior piezoelectric properties in potassium–sodium niobate lead-free ceramics. Adv Mater 28:8519–8523
16. Wu B, Wu H, Wu J, Xiao D, Zhu J, Pennycook SJ (2016) Giant piezoelectricity and high Curie temperature in nanostructured alkali niobate lead-free piezoceramics through phase coexistence. J Am Chem Soc 138:15459–15464
17. Wang X, Wu J, Xiao D, Zhu J, Cheng X, Zheng T, Zhang B, Lou X, Wang X (2014) Giant piezoelectricity in potassium–sodium niobate lead-free ceramics. J Am Chem Soc 136:2905–2910

18. Lv X, Zhu J, Xiao D, Zhang X, Wu J (2020) Emerging new phase boundary in potassium sodium-niobate based ceramics. Chem Soc Rev 49:671–707
19. Hu Q, Du H, Feng W, Chen C, Huang Y (2015) Studying the roles of Cu and Sb in $K_{0.48}Na_{0.52}NbO_3$ lead-free piezoelectric ceramics. J Alloys Compd 640:327–334
20. Kong Z, Bai W, Zheng P, Zhang J, Wen F, Chen D, Shen B, Zhai J (2017) Enhanced electromechanical properties of $CaZrO_3$-modified $(K_{0.5}Na_{0.5})NbO_3$-based lead-free ceramics. Ceram Int 43:7237–7242
21. Huang T, Xiao D, Liu C, Li F, Wu B, Wu J, Zhu J (2014) Effect of $SrZrO_3$ on phase structure and electrical properties of $0.974(K_{0.5}Na_{0.5})NbO_3$–$0.026Bi_{0.5}K_{0.5}TiO_3$ lead-free ceramics. Ceram Int 40:2731–2735
22. Liu C, Xiao D, Huang T, Wu J, Li F, Wu B, Zhu J (2014) Composition induced rhombohedral–tetragonal phase boundary in $BaZrO_3$ modified $(K_{0.445}Na_{0.50}Li_{0.055})NbO_3$ lead-free ceramics. Mater Lett 120:275–278
23. Wang R, Bando H, Kidate M, Nishihara Y, Itoh M (2011) Effects of Effects of A-site ions on the phase transition temperatures and dielectric properties of $(1 - x)(Na_{0.5}K_{0.5})NbO_3 - x$AZrO3. Jpn J Appl Phys 50:09
24. Chen Y, Xue D, Ma Y, Liu K, Chen Z, Jiang X (2016) Phase transitional behavior and electrical properties of $(1–x)(K_{0.475}Na_{0.48}Li_{0.05})Nb_{0.95}Sb_{0.05}O_3 - xCaZrO_3$ lead-free ceramics. Phys Lett A 380:2974–2978
25. Zhang B, Wu J, Cheng X, Wang X, Xiao D, Zhu J, Wang X, Lou X (2013) Lead-free piezoelectrics based on potassium–sodium niobate with giant d_{33}. ACS Appl Mater Interfaces 5:7718–7725
26. Gou Q, Zhu J, Wu J, Li F, Jiang L, Xiao D (2018) Microstructure and electrical properties of $(1–x)K_{0.5}Na_{0.5}NbO_3$–$xBi_{0.5}Na_{0.5}Zr_{0.85}Sn_{0.15}O_3$ lead-free ceramics. J Alloy Compd 730:311–317
27. Zhang B, Wang X, Cheng X, Zhu J, Xiao D, Wu J (2013) Enhanced d_{33} value in $(1–x)[(K_{0.50}Na_{0.50})_{0.97}Li_{0.03}Nb_{0.97}Sb_{0.03}O_3]$–$xBaZrO_3$ lead-free ceramics with an orthorhombic–rhombohedral phase boundary. J Alloy Compd 581:446–451
28. Igathinathane C, Pordesimo LO, Columbus EP, Batchelor WD, Methuku SR (2008) Shape identification and particles size distribution from basic shape parameters using ImageJ. Comput Electron Agr 63:168–182
29. Yu Y, Li J, Dai X, Yi Y, Pan Y, He C, Liu Y, Liu X, Chen Y (2019) Composition-driven phase evolution and piezoelectric properties of $(1 - x)(K_{0.48}Na_{0.52})_{0.96}Li_{0.04}Nb_{0.95}Sb_{0.05}O_3 - x$Bi0.5(Na0.84K0.16)0.48Ba0.02ZrO3 lead-free ceramics. Mater Res Express 6:106322
30. Liu Y, Ding Y, Du X, Shi M, He C, Li J, Dai X, Xu Z, Chen Y (2019) Evolution of phase structure, microstructure and piezoelectric properties in $(1–x)(K_{0.4}Na_{0.6})Nb_{0.96}Sb_{0.04}O_3 - xCa_{0.1}(Bi_{0.5}K_{0.5})_{0.9}ZrO_3$ lead-free ceramics. J Mater Sci Mater Electron 30:17856–17862
31. Uchino K, Nomura S (1982) Critical exponents of the dielectric constants in diffused-phase-transition crystals. Ferroelectrics 44:55–61
32. Rivera I, Kumar A, Ortega N, Katiyar RS, Lushnikov S (2009) Divide line between relaxor, diffused ferroelectric, ferroelectric and dielectric. Solid State Commun 149:172–176
33. Xu G, Shirane G, Copley JRD, Gehring PM (2004) Neutron elastic diffuse scattering study of $Pb(Mg_{1/3}Nb_{2/3})O_3$. Phys Rev B 69:064112
34. Hirota K, Ye ZG, Wakimoto S, Gehring PM, Shirane G (2002) Neutron diffuse scattering from polar nanoregions in the relaxor $Pb(Mg_{1/3}Nb_{2/3})O_3$. Phys Rev B 65:104105
35. Chen T, Wang H, Zhang T, Wang G, Zhou J, Zhang J, Liu Y (2013) Piezoelectric behavior of $(1–x)K_{0.50}Na_{0.50}NbO_3$ – $xBa_{0.80}Ca_{0.20}ZrO_3$ lead-free ceramics. Ceram Int 39:6619–6622